Mon. Not. R. Astron. Soc. **345,** 834–846 (2003)

A Whole Earth Telescope campaign on the pulsating subdwarf B binary system PG 1336−018 (NY Vir)

D. Kilkenny,[1⋆] M. D. Reed,[2,3] D. O'Donoghue,[1] S. D. Kawaler,[3] A. Mukadam,[4] S. J. Kleinman,[3,5] A. Nitta,[4,5] T. S. Metcalfe,[4,6] J. L. Provencal,[7] T. K. Watson,[8] D. J. Sullivan,[9] T. Sullivan,[9] R. Shobbrook,[10] X. J. Jiang,[11] S. Joshi,[12] B. N. Ashoka,[13] S. Seetha,[13] E. Leibowitz,[14] P. Ibbetson,[14] H. Mendelson,[14] E. Meištas,[15] R. Kalytis,[15] D. Ališauskas,[16] P. Martinez,[1] F. van Wyk,[1] R. S. Stobie,[1] F. Marang,[1] S. Zola,[17] J. Krzesinski,[18] W. Ogloza,[18] P. Moskalik,[19] R. Silvotti,[20] A. Piccioni,[21] G. Vauclair,[22] N. Dolez,[22] M. Chevreton,[23] S. Dreizler,[24] S. L. Schuh,[24] J. L. Deetjen,[24] J.-E. Solheim,[25] J. M. Gonzalez Perez,[25] A. Ulla,[26] R. Østensen,[27] M. Manteiga,[28] O. Suarez,[28] M. Burleigh,[29] S. O. Kepler,[30] A. Kanaan[31] and O. Giovannini[32]

[1]*South African Astronomical Observatory, PO Box 9, Observatory 7935, South Africa*
[2]*Department of Physics, Astronomy and Material Science, SW Missouri State University, 901 S. National, Springfield, MO 65804, USA*
[3]*Department of Physics and Astronomy, Iowa State University, Ames IA50011, USA*
[4]*Department of Astronomy, University of Texas, Austin, TX 78712, USA*
[5]*Apache Point Observatory, PO Box 59, Sunspot, NM 88349, USA*
[6]*Harvard-Smithsonian Centre for Astrophysics, 60, Garden St., Cambridge MA 02138, USA*
[7]*University of Delaware, Newark, DE 19716, USA*
[8]*Southwestern University, 1001 E. University Avenue, Georgetown, Texas 78626, USA*
[9]*School of Chemical and Physical Sciences, Victoria University of Wellington, PO Box 600, Wellington, New Zealand*
[10]*Chatterton Astronomy Department, School of Physics, University of Sydney, NSW 2006, Australia*
[11]*National Astronomical Observatories, Chinese Academy of Sciences, Beijing 100012, China*
[12]*State Observatory, Manora Peak, Naini Tal 263 129, India*
[13]*Indian Space Research Organisation, Airport Road, Vimanapura, Bangalore 560 017, India*
[14]*Wise Observatory, Tel-Aviv University, Tel-Aviv 69978, Israel*
[15]*Institute of Theoretical Physics and Astronomy, Goštauto 12, Vilnius 2600, Lithuania*
[16]*Institute of Materials Research and Applied Sciences, Vilnius University, Čiurlionio 29, Vilnius 2009, Lithuania*
[17]*Astronomical Observatory, Jagiellonian University, ul. Orla 171, 30–244 Kraków, Poland*
[18]*Mt. Suhora Observatory, Kraków Pedagogical University, ul. Podchorçżych 2, Kraków, Poland*
[19]*Nicolas Copernicus Astronomical Centre, ul. Bartycka 18, 00-716 Warszawa, Poland*
[20]*Osservatorio Astronomico di Capodimonte, Via Moiariello 16, I-80131, Napoli, Italy*
[21]*Dipartimento di Astronomia, Università di Bologna, Via Ranzani 1, I–40127 Bologna, Italy*
[22]*Université Paul Sabatier, Observatoire Midi-Pyrénées, CNRS/UMR5572, 14 av. E. Belin, 31400 Toulouse, France*
[23]*Observatoire de Paris-Meudon, DAEC, 92195, Meudon, France*
[24]*Institut für Astronomie und Astrophysik, Universität Tübingen, Sand 1, D–72076 Tübingen, Germany*
[25]*Institutt for Fysikk, Universitetet i Tromsø N-9037, Tromsø, Norway*
[26]*Universidade de Vigo, Depto. de Fisica Aplicada, Facultade de Ciencias, Campus Marcosende-Lagoas, 36200 Vigo, Spain*
[27]*Isaac Newton Group of Telescopes, E–37800 Santa Cruz de La Palma, Canary Islands, Spain*
[28]*Depto. de Ciencias de la Navegación y de la Tierra E.S. Marina, Civil. Univ. de Coruña, Paseo de Ronda 51, E-15011 A, Coruña, Spain*
[29]*Department of Physics and Astronomy, University of Leicester, Leicester LE1 7RH*
[30]*Instituto de Fisica, UFRGS, 91501-900, Porto Alegre, RS, Brazil*
[31]*Universidade Federal de Santa Catarina, Florianópolis, SC, Brazil*
[32]*Departamento de Física e Química, Universidade de Caxias do Sul, CEP 95001-970, Caxias do Sul, RS, Brazil*

Accepted 2003 July 7. Received 2003 July 7; in original form 2002 October 18

ABSTRACT

We present results from a multisite ('Whole Earth Telescope') photometric campaign on PG 1336−018, the close eclipsing binary system containing a pulsating subdwarf B (sdB) star. The main part of the campaign (1999 April) resulted in ∼172 h of observations, representing

⋆E-mail: dmk@saao.ac.za

a coverage of about 47 per cent, and additional data were obtained outside the core campaign. Periodogram analysis shows that the light variations are dominated by three frequencies near 5757, 5585 and 5369 μHz (∼174, 179 and 186 s, respectively), although many frequencies are present, particularly in the range 5000–6000 μHz (∼200–170 s). We identify, with some confidence, 28 frequencies down to a semi-amplitude of 0.0005 in fractional intensity (equivalent to about 0.5 mmag). It is clear that the pulsation frequencies of PG 1336−018 have changed substantially since the 1996 discovery observations were made, and that amplitude changes occur, at least in the dominant three frequencies, on relatively short time-scales (of the order of a day). On the assumption that the pulsating star is phase-locked in the binary system, we have searched for rotational splitting of frequencies near the orbital and half of the orbital period, but the results are confused by aliasing at those frequencies (due to the data gaps caused by the eclipses). A preliminary model qualitatively matches the distribution of frequencies in PG 1336−018, with some good individual correspondences, but cannot be considered adequate because geometric cancellation should hide some of the modes which are apparently detected. Analysis of the pulsations during eclipse recovers three of the strongest modes, but the limited eclipse data – which can, at best, be only about 9 per cent of the total – do not allow mode identification at this stage. Simulations indicate that an overall coverage of about 80 per cent would be required for this to be viable. An attempt was made to determine phase shifts in the pulsation frequencies as a way of directly measuring the size of the binary orbit, but the uncertainties in the method are comparable to the light travel time across the orbit (probably less than a second).

Key words: stars: individual: PG 1336−018 – stars: oscillations – stars: variables: other.

1 INTRODUCTION

The rapidly pulsating subdwarf B (sdB) stars are a recently discovered class of variable star. They are generally multiperiodic, probably pulsating in low-order radial and non-radial p-modes, with periods mainly in the range 100–200 s, and amplitudes typically ∼0.01 mag. Some, but not all, of them show spectroscopic evidence for a late-type (F–G) companion and, although little is known about the binary orbits of the pulsators (with one notable exception – the subject of this paper), it is likely that the stars in each binary are well separated. The pulsating sdB stars have been dubbed 'EC14026' stars following the tradition of using the prototype (EC14026−2647) to name a class of stars, but have also been referred to as sdBV stars by analogy with the pulsating white dwarf stars (DAV, DBV). Recent reviews of observational and theoretical studies of pulsating sdB stars have been given by Charpinet, Fontaine & Brassard (2001) and Kilkenny (2002), for example.

A possible driving mechanism for the observed pulsations has been suggested by Charpinet et al. (1997) who find that local enhancement of the iron abundance can occur due to diffusive equilibrium between gravitational settling and radiative levitation. The locally increased iron abundance creates an 'opacity bump' which then drives pulsation via the κ mechanism. They find that radial and non-radial pulsations can be driven for $29\,000 < T_{\rm eff} < 36\,500$ K in representative models with $M = 0.48\ {\rm M}_{\odot}$ and $\log g = 5.8$. A very good review of this work was recently given by Charpinet et al. (2001).

At the time of writing, mode identification for the sdB pulsators is in its infancy – although a promising new approach has been described by Charpinet, Fontaine & Brassard (2002) – but because multimode pulsations are potentially very valuable as diagnostics of the internal structure of sdB stars and because some of the EC14026 stars clearly exhibit *many* pulsation modes, it is desirable to obtain intensive, multisite photometric monitoring of selected stars to separate and identify the frequencies present; such campaigns have already been carried out for a few stars. For PB8783, O'Donoghue et al. (1998) found at least 12 and possibly 15 frequencies which could be qualitatively identified with low-order radial and non-radial modes in a model with appropriate $T_{\rm eff}$ and $\log g$. For PG 1605+072, the largest amplitude and longest period pulsator in this class (periods ∼200–600 s, amplitudes up to ∼0.3 mag), Kilkenny et al. (1999) found over 50 frequencies with semi-amplitudes greater than 0.0006 mag. A multisite campaign for PG 1047+003 (Kilkenny et al. 2002) identified 18 frequencies between 5700 and 9605 μHz (175–104 s), doubling the number of known frequencies and with indications from several frequency spacings near 1.05 μHz that the rotation period of the star is ∼11 d.

In this paper we present results for a 'Whole Earth Telescope' (WET)[1] campaign on the pulsating sdB star, PG 1336−018, which was detected as a hot subdwarf by the Palomar–Green survey (Green, Schmidt & Liebert 1986) and shown to be a close eclipsing binary by Kilkenny et al. (1998). PG 1336−018, now officially named NY Vir (Kazarovets, Samus & Durlevich 2000), is remarkably similar to the binary HW Vir (Menzies & Marang 1986; Wood, Zhang & Robinson 1993) except that the sdB primary in HW Vir is not known to pulsate. A third 'HW Vir' system with well-determined orbital parameters, HS 0705+6700, also containing a non-pulsating sdB star, has very recently been discovered by Drechsel et al. (2001).

From the work by Kilkenny et al. (1998), PG 1336−018 appears to consist of a hot subdwarf primary ($T_{\rm eff} = 33\,000 \pm 1000$ K, $\log g = 5.7 \pm 0.1$) and a ∼M5 main-sequence secondary ($T_{\rm eff} \sim 3000$ K).

[1] For further details, see http://wet.iitap.iastate.edu

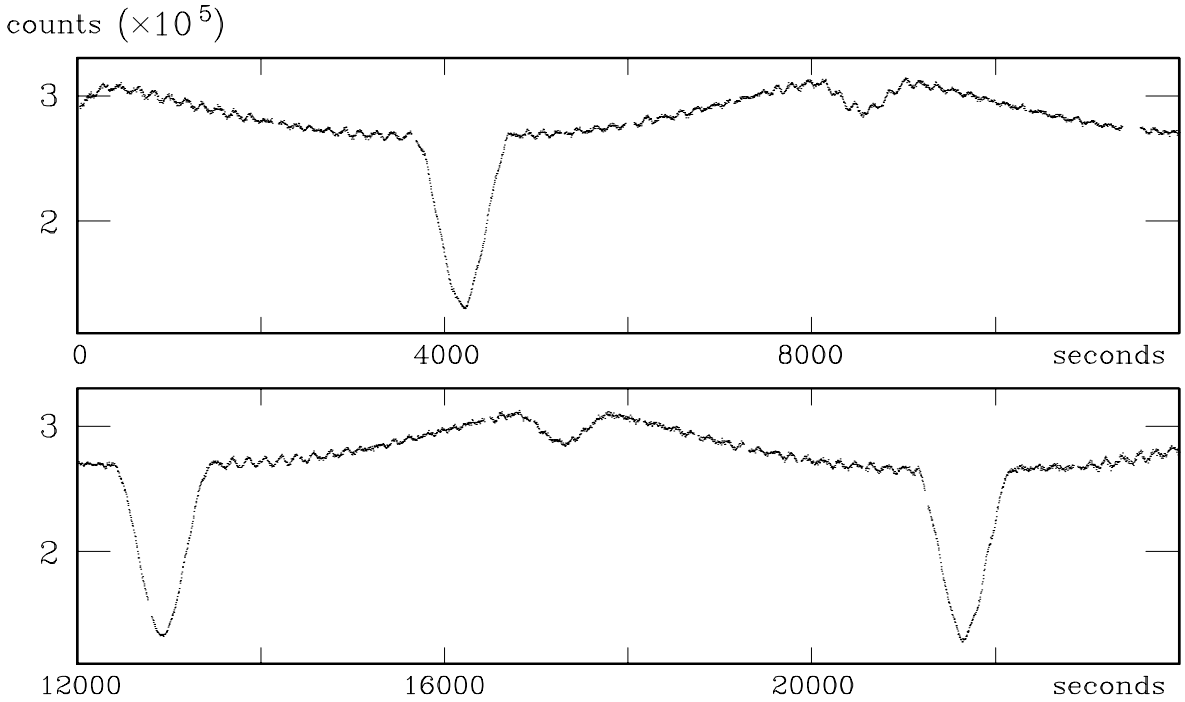

Figure 1. Most of a single run (fvw192) from one of the sites; integration times are 5 s. The ordinate is in units of 10^5 counts (per 5 s) corrected for sky background and atmospheric extinction. The abscissa is time in seconds from the start of the run. The largest pulsation variations visible (e.g. after the first eclipse in the bottom panel) are less than 3 per cent (peak to peak) of the total light intensity. Note the clear beating of the pulsations and that the pulsations are very obvious in secondary eclipse and can also be seen as asymmetries in at least two of the primary eclipses, even though the pulsating star is substantially occulted by the cool companion.

Although the two stars are well separated, each with a radius of ∼20 per cent of their separation, their actual radii are only about 0.17 $R_\odot$, so that their separation is less than 1 $R_\odot$ and the orbital period is extremely short at 0.101016 d (Kilkenny et al. 2000). A substantial 'reflection' effect is thus seen in the out-of-eclipse part of the light curve, due to the large temperature difference between the primary and secondary stars. The discovery paper found two clear pulsation frequencies in the sdB star, with periods near 184 and 141 s and semi-amplitudes of ∼0.01 and ∼0.005 mag, respectively. There were also weak indications that there might be more frequencies present with amplitudes $\leqslant$0.003 mag.

The combination of eclipses, reflection effect and multiperiodic pulsation produces a stunning light curve for the system. A sample is shown in Fig. 1, which is most of a single run of good quality data from one of the sites involved in the current campaign. The frequency beating is very obvious in the figure and pulsations are clearly visible during secondary eclipses. It is also clear that the primary eclipses show asymmetries due to the fact that pulsations still have some effect on the light curve even when the pulsating primary star is substantially occulted by the cool secondary. This was not unambiguously evident in the discovery data (Kilkenny et al. 1998) although some effort was made to detect such an effect.

For PG 1336−018, the aims of the campaign were as follows.

(i) To resolve, as fully as possible, the stellar pulsation frequencies by searching for additional low-amplitude modes already suspected to be present in the discovery data.

(ii) To search for rotational splitting of the principal frequencies. It is reasonable to expect, in such a close binary, that the rotation of the components will be phase-locked to the orbital motion. Detection of rotational splitting would help with pulsation mode identification.

(iii) To create a model which will match the observed frequencies – again as a way of identifying pulsation modes.

(iv) To attempt to model light variations during primary eclipse when the pulsating sdB component is significantly occulted and to compare these with out-of-eclipse variations. This is difficult to do but would, in principle, allow identification of the pulsation modes.

(v) To look for phase shifts in pulsation frequencies as a way of directly measuring the orbital size. This was tried with the discovery data (Kilkenny et al. 1998) which were too sparse to give significant results (the light travel time across the orbit is only ∼0.9 s). With the WET data, a more complete solution of the pulsation frequencies might allow the orbital phase shifts to be detected.

2 OBSERVATIONS

Telescope time for time series photometry of PG 1336−018 was allocated at the following observatories (telescopes and instruments in parenthesis) during 1999 April: Observatorio do Pico dos Dias (Itajubá), Brazil (0.6-m telescope + CCD detector); Beijing Astronomical Observatory, China (0.85-m and 2.16-m + three-channel photoelectric photometers); Observatoire du Pic du Midi, France (2-m + three-channel); Uttar Pradesh State Observatory, Naini Tal, India (1-m + three-channel); Wise Observatory, Israel (1-m + 2-channel); Osservatorio di Bologna, Loiano, Italy (1.5-m + 2-channel); Moletai Observatory, Lithuania (1.65-m + three-channel); Mt. John Observatory, New Zealand (1-m + three-channel); Mt. Suhora Observatory, Poland (0.6-m + three-channel); Siding Spring Observatory (1-m + three-channel); South African Astronomical Observatory, Sutherland (1.9-m + 1-channel; 0.75-m + CCD); Calar Alto Observatory, Spain (1.2-m + CCD); Tenerife

Observatory, Spain (0.8-m + three-channel); and McDonald Observatory, Texas, USA (2.1-m + three-channel).

The WET campaign (Xcov17) on PG 1336−018 was planned to run during 1999 April 7–21, although some sites were able to obtain data before and after the main campaign. Table 1 gives a listing of all the individual runs obtained during 1999 April 3–21 and Table 2 lists the other runs. Fig. 2 shows the coverage for the main campaign data. The actual data are plotted in the figure, with the eclipses and reflection effect variations removed (see Section 3).

The WET campaigns are designed to obtain continuous coverage of a selected object for typically two weeks. Usually, two or more sites can access a principal target at any one time; this redundancy compensates for bad weather or instrumental problems (for example) at any given site. In Xcov17, however, there were two principal targets, PG 1336−018 and BPM37093. The latter is very much a southern hemisphere object ($\delta \sim -50^{\circ}$) and so had priority from southern sites, leaving something of a gap in the Pacific Ocean region – about 3 h between McDonald and Beijing Astronomical Observatories, even when conditions were photometric at both sites. Thus, the Xcov17 coverage was not as continuous as might have been wished. Despite this, the 14 days of the 'core' campaign resulted in about 172 h of observations, or about 47 per cent coverage. Including all the data in Table 1, ∼206 h of data were obtained (at 43 per cent coverage).

Because PG 1336−018 is relatively bright (*B* magnitude outside eclipse varies between about 13.3 and 13.5) and because most of the telescopes used were of 1-m to 2-m class, it was decided to use 5-s integrations wherever possible. This gives good time resolution and counts of the order of 10^5 per integration – sufficient for high-accuracy photometry (see Fig. 1).

3 DATA REDUCTION

The reduction of the photoelectric data was carried out on each individual run using standard techniques (see, for example, Nather et al. 1990). For the three-channel data, the smoothed sky counts were subtracted from the stellar data on a point-by-point basis; for the other data, the less frequent sky measures were linearly interpolated and subtracted from each star measure. The sky counts were sufficiently small compared to star counts and measures of the sky background were sufficiently frequent that this procedure was perfectly adequate.

For each run, the mean extinction coefficient which best 'flattened' the data was determined and applied. In addition, as different sites, instrument sensitivities and telescope apertures result in different mean light-curve levels, each light curve was normalized by its own mean level, yielding data in fractional intensity units, $\Delta I/I$. Winget et al. (1994) have called this unit the 'modulation intensity', or mi. One thousandth of an mi is then a 'milli modulation intensity' (mmi) which is related by a scaling factor, 1.0857, to the more conventional mmag unit; the latter is, however, logarithmic in the measured light intensity whereas the mi is linear. We shall adopt the mi (or mmi) throughout the analysis.

To investigate the pulsation spectrum of the sdB component, it is necessary to remove the very obvious orbital contributions to the light curve. The eclipses were snipped out of the data and the out-of-eclipse reflection effect was removed by subtracting a two-sinusoid fit to the data. This is simply an empirical treatment which seems to work very well; we do not imply any physical meaning to the two sinusoids.

During Xcov17, results were obtained at three sites using CCDs. Data were received from the Nordic Optical Telescope (NOT) and

Table 1. Log of Xcov17 high-speed photometry of PG 1336−018.

Run name	Date 1999	Start (UT)	Run (h)	Observatory	Tel (m)
capg1336r1	Apr 3	04:17:24	0.7	Calar Alto	1.2
capg1336r2	Apr 3	22:06:29	6.8	Calar Alto	1.2
capg1336r3	Apr 4	21:00:04	8.1	Calar Alto	1.2
eml-001	Apr 5	19:29:11	0.6	Wise	1.0
capg1336r4	Apr 5	20:40:28	8.3	Calar Alto	1.2
capg1336r5	Apr 6	20:26:06	8.7	Calar Alto	1.2
capg1336r6	Apr 7	21:28:00	7.6	Calar Alto	1.2
iza-002	Apr 8	04:37:50	1.6	Tenerife	0.8
capg1336r7	Apr 8	21:28:00	9.2	Calar Alto	1.2
iza-003	Apr 8	22:54:50	5.9	Tenerife	0.8
jxj-9902	Apr 9	13:06:40	7.3	Beijing AO	0.85
suh73	Apr 9	19:42:30	7.1	Mt. Suhora	0.6
capg1336r9	Apr 9	20:40:00	4.6	Calar Alto	1.2
iza-004	Apr 9	21:46:50	8.1	Tenerife	0.8
capg1336r10	Apr 10	00:25:45	4.7	Calar Alto	1.2
capg1336r11	Apr 10	20:52:00	2.4	Calar Alto	1.2
lo1004	Apr 10	22:30:00	5.0	Loiano	1.5
iza-005	Apr 10	22:41:30	7.0	Tenerife	0.8
pm1003	Apr 10	22:42:50	0.4	Sutherland	1.9
pm1004	Apr 10	23:30:30	1.5	Sutherland	1.9
capg1336r12	Apr 11	00:46:00	5.1	Calar Alto	1.2
tkw-0060	Apr 11	04:30:00	5.2	McDonald	2.1
iza-006	Apr 11	21:52:50	5.4	Tenerife	0.8
pm1007	Apr 11	22:07:20	7.6	Sutherland	1.9
tkw-0061	Apr 12	06:27:30	1.5	McDonald	2.1
jxj-9903	Apr 12	13:49:50	7.3	Beijing AO	0.85
suh74	Apr 12	18:55:40	1.7	Mt. Suhora	0.6
eml-004	Apr 12	18:56:40	1.8	Wise	1.0
pm1008	Apr 12	21:00:00	6.8	Sutherland	1.9
iza-007	Apr 12	22:30:50	7.0	Tenerife	0.8
jxj-9904	Apr 13	13:10:30	6.1	Beijing AO	0.85
n49-0416	Apr 13	17:12:00	5.7	Naini Tal	1.0
capg1336r14	Apr 13	21:32:45	1.3	Calar Alto	1.2
iza-008	Apr 13	21:34:20	7.9	Tenerife	0.8
tkw-0062	Apr 14	08:22:00	0.6	McDonald	2.1
n49-0417	Apr 14	17:17:30	5.6	Naini Tal	1.0
suh76	Apr 14	19:18:10	7.0	Mt. Suhora	0.6
fvw187	Apr 14	22:13:36	1.9	Sutherland	1.9
fvw188	Apr 15	01:24:50	1.8	Sutherland	1.9
jxj-9905	Apr 15	12:58:40	7.0	Beijing AO	0.85
suh77	Apr 15	19:10:50	1.8	Mt. Suhora	0.6
n49-0418	Apr 15	19:38:50	1.7	Naini Tal	1.0
fvw190	Apr 15	22:27:30	3.5	Sutherland	1.9
suh78	Apr 15	22:47:50	3.9	Mt. Suhora	0.6
tkw-0061	Apr 16	03:41:30	5.9	McDonald	2.1
lo1604	Apr 16	19:57:52	5.3	Loiano	1.5
jlp-0160	Apr 17	04:36:00	6.4	McDonald	2.1
fvw192	Apr 17	21:34:30	7.3	Sutherland	1.9
jlp-0162	Apr 18	03:58:20	7.3	McDonald	2.1
jxj-9907	Apr 18	15:17:30	3.4	Beijing AO	0.85
jlp-0164	Apr 19	05:45:00	1.6	McDonald	2.1
jlp-0165	Apr 19	07:29:15	3.6	McDonald	2.1
ap1999q2	Apr 19	10:38:50	1.0	Mt. John	1.0
ap1999q3	Apr 19	11:36:30	2.6	Mt. John	1.0
n49-0420	Apr 19	17:21:30	3.9	Naini Tal	1.0
edroda04	Apr 19	20:41:40	4.4	Moletai	1.65
n49-0422	Apr 20	16:47:10	4.6	Naini Tal	1.0
ita200499pg	Apr 21	01:43:00	1.6	Itajuba CCD	0.6
jlp-0167	Apr 21	03:28:20	4.5	McDonald	2.1
jlp-0168	Apr 21	08:10:29	2.9	McDonald	2.1

Table 2. Log of other high-speed photometry of PG 1336−018.

Run name	Date 1999	Start (UT)	Run (h)	Observatory	Tel (m)
mdr019	Mar 8	10:30:00	1.6	McDonald	2.1
mdr028	Mar 14	06:48:00	4.7	McDonald	2.1
mdr031	Mar 17	04:48:00	4.6	McDonald	0.9
mdr032	Mar 18	09:30:00	2.5	McDonald	0.9
mdr034	Mar 19	04:34:00	7.5	McDonald	0.9
mdr036	Mar 20	08:29:00	3.6	McDonald	0.9
ma2099q2	Mar 20	13:42:00	3.8	Mt. John	1.0
mdr038	Mar 22	03:53:30	8.0	McDonald	0.9
mdr040	Mar 23	08:08:00	1.3	McDonald	0.9
notpg1136r1	May 2	22:27:32	6.6	Nordic	2.6

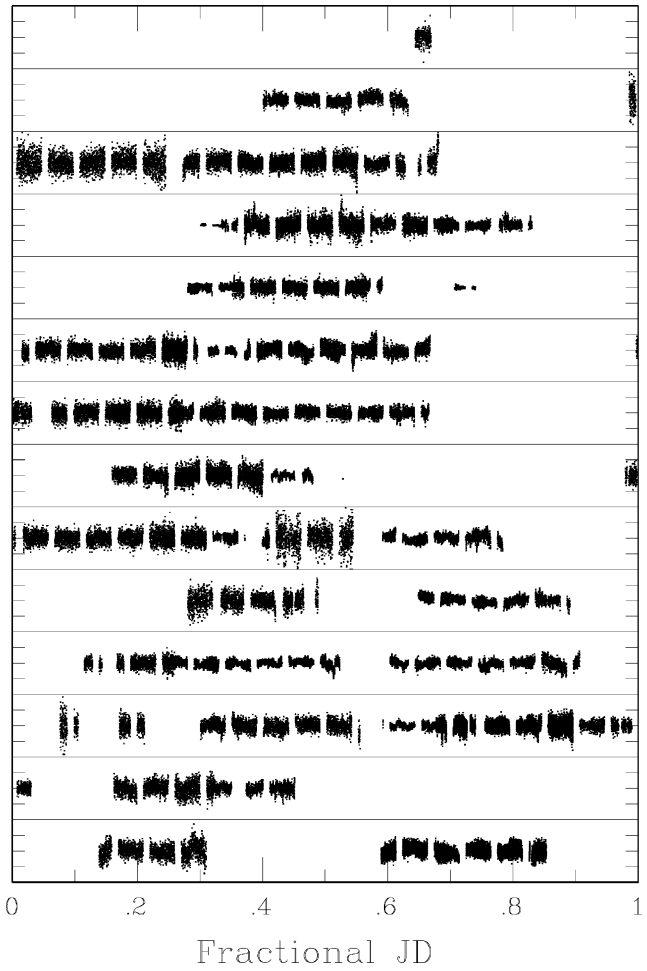

Figure 2. Coverage diagram for the Xcov17 campaign on PG 1336−018. Each panel represents one day and the panels read left-to-right and top-to-bottom. The panels are 0.2 mi in height so that the ordinate carets are separated by 0.05 mi (fractional intensity units; see Section 3). The actual data are plotted, although on a very compressed scale, with the eclipses and reflection effect variations removed.

Itajuba Observatory in the standard WET format and data reduction proceeded as above. The NOT uses windowing software to read out the CCD which results in a dead time of only about 1 s, whilst Itajuba used a frame-transfer CCD, making observations with the required sampling interval of 5 s easily attainable. Data from Calar Alto were received as differential photometry but, as any comparison stars will

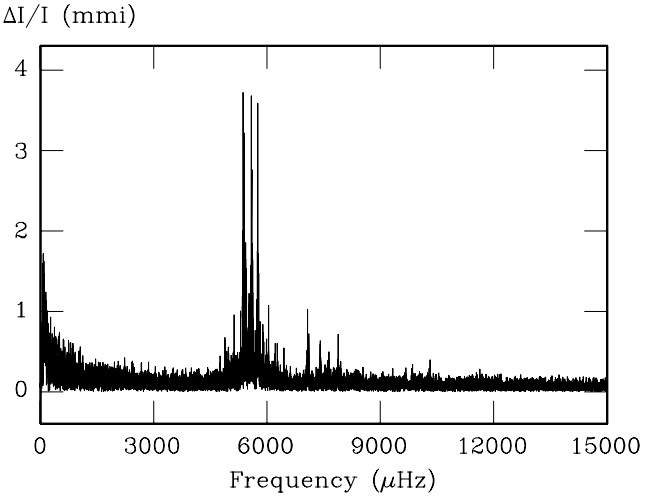

Figure 3. Periodogram (amplitude/frequency) for the data in Fig. 2. Amplitude units are fractional intensity ($\Delta I/I$) in thousandths or mmi units. The frequency range plotted is equivalent to periods down to 67 s.

probably be significantly redder than PG 1336−018, differential extinction across the CCD can introduce small non-linear 'drifts' into the reduced data. After correcting for the eclipses and reflection effect, any remaining trends were removed using second-order to fourth-order polynomials (this assumes that any low-frequency variations are produced by residual sky or instrumental effects rather than by the star). A further problem was encountered with the Calar Alto data because CCD detectors are generally used for 'deep' imaging, where very precise timekeeping is usually unnecessary. The data acquisition software was not linked to a highly accurate time service such as the GPS network and consequently small errors might accumulate over the course of a long run on a given night. (All sites were checked near the start of each observing run to be synchronized to better than 1 s with time from the US Naval Observatory, even though nearly all sites have access to the GPS network.) However, careful checks using the phases of the pulsational variations and analyses with and without the Calar Alto data have convinced us that these are consistent with the rest of the data.

The Xcov17 data, reduced and corrected as described above, are displayed in a very condensed form in Fig. 2 with the corresponding periodogram covering the range $0 < f < 15\,000$ μHz shown in Fig. 3. The latter is also on a rather small scale, but serves to show that virtually all of the signal is between about 4000 and 9000 μHz and, in what follows, we have concentrated (although not exclusively) on this frequency range.

4 FREQUENCY ANALYSIS

Because the detection of many modes of pulsation provides the possibility of investigating the internal structure of stars (see, for example, Winget et al. 1991), the first aim of the multisite campaign was to resolve and accurately measure as many frequencies as possible. The frequency analyses described in this section were all carried out using periodogram analysis following the method of Deeming (1975) as modified by Kurtz (1985).

4.1 Xcov17 photoelectric data in halves

Formally, the Fourier transform is a transformation of the light curve and all peaks do not represent physical pulsation modes. The presence of the same significant peaks in two data sets – or two separate

subsets of the full data set – strengthens their identification as physical modes. So, as a first step, the photomultiplier data from the two-week Xcov17 campaign were divided into two 'halves' of about 6 d each (the first day and a half of the actual campaign produced very little data for PG 1336−018, due to poor weather conditions; see Fig. 2). Periodograms were calculated for each data subset in the range $3500 < f < 9500$ μHz (periods between about 285 and 105 s, respectively). The frequency with the largest amplitude in each periodogram was removed by a least-squares procedure (Deeming 1968) which calculated the best-fitting amplitude and phase for the given frequency and subtracted the resulting sine wave from each data set. New periodograms were then recomputed based on the revised data sets. This procedure was repeated until the 20 frequencies with largest amplitude had been removed. A comparison of the two sets of results showed 14 frequencies which agreed very well ($\Delta f <$ 0.4 μHz) between the two halves of the data. The next step was to remove these 14 frequencies simultaneously from both data subsets, using a Taylor expansion non-linear least-squares technique, and then to calculate individually the next 20 frequencies, from which five more close matches were found.

Fig. 4 shows the window functions for the two data subsets. The very obvious alias patterns have a frequency separation at ∼230 μHz, or a periodicity of ∼0.05 d, and are clearly caused by the gaps in the data where the two eclipses per orbital period (0.101016 d) have been removed. Present, although not so clear in the figure, are the alias patterns with 11.57 μHz separation – the 1-d aliases. Fig. 5 shows the periodograms, with no frequency removal (or 'pre-

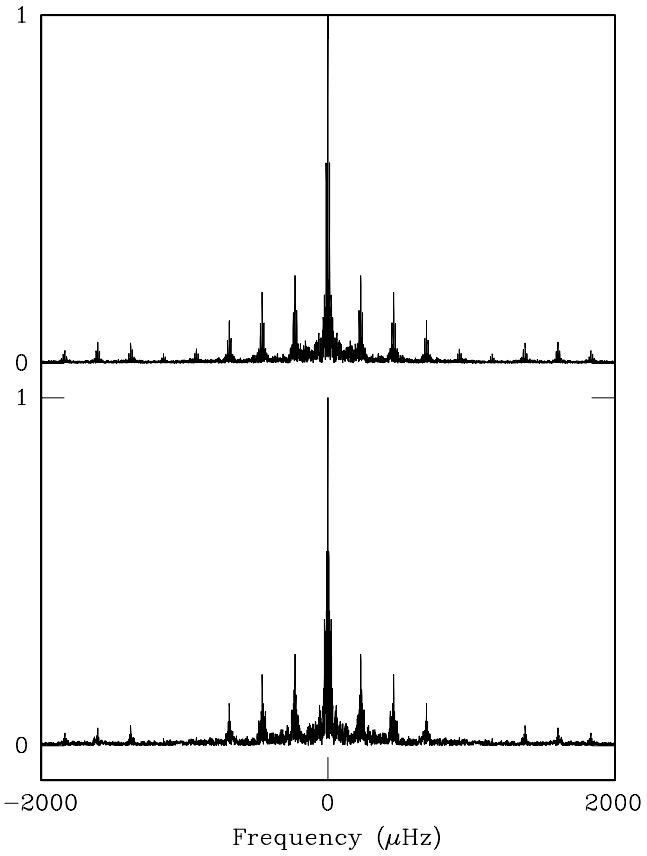

Figure 4. Window functions for the first (upper) and second (lower) halves of the Xcov17 photomultiplier data. The functions are normalized to unity at zero frequency. The very obvious aliasing ($\Delta f \sim 230$ μHz) is due to the regular gaps in the data where the eclipses have been removed. The effect of the 1-d alias patterns ($\Delta f \sim 11.57$ μHz) is just discernible.

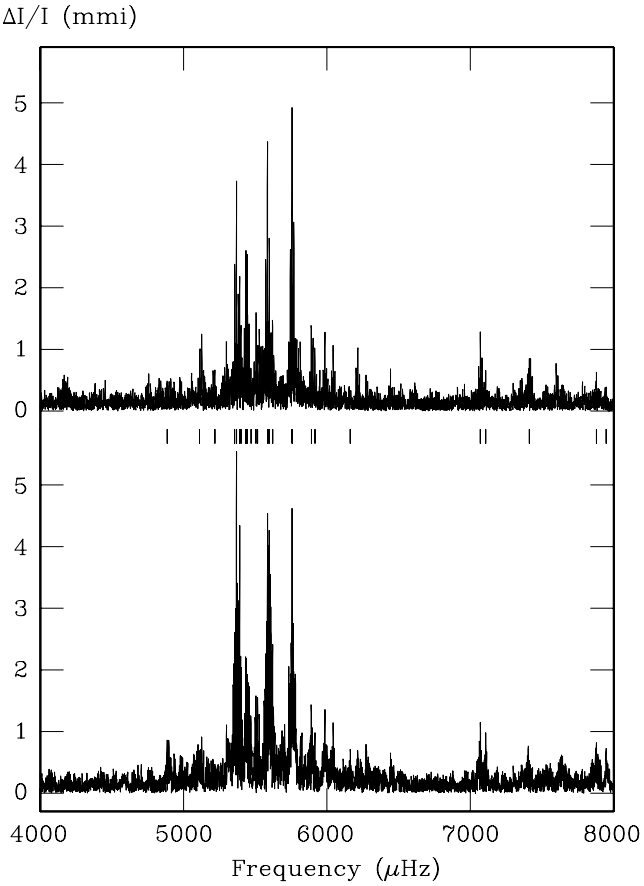

Figure 5. Periodograms (amplitude/frequency) for the first (upper) and second (lower) halves of the Xcov17 photomultiplier data. Amplitude units are fractional intensity ($\Delta I/I$) in thousandths or mmi units. The small vertical lines in the middle of the figure indicate 27 of the 28 frequencies extracted from the full data set (the other frequency is off the figure at 10 315 μHz). See Table 4 for a full listing.

whitening') for the same data. Note the occurrence of corresponding peaks, even at low amplitude, in the two plots. As an example, Fig. 6 shows the periodograms for the data after the removal of 19 frequencies. The noise is at about the 0.2-mmi level, and it appears that even after subtraction of 19 frequencies, there is still significant power at several frequencies in both periodograms, especially in the 7000–8000 μHz range (∼140–125 s). Consequently, as a third iteration, the first 19 frequencies were simultaneously removed from the data and the next 30 strongest frequencies determined individually. This reached down to amplitudes of ∼0.4 mmi and revealed four further matches.

The two data subsets were also analysed in the frequency ranges $500 < f < 3500$ μHz and $9500 < f < 30\,000$ μHz (so that, together with the analysis described above, the period range 33–2000 s was covered). No significant power was found in the low-frequency range, given that slow changes are as likely to be artefacts of the reduction processes as variations in the star. In the high-frequency range, one frequency was identified in both the 'a' and 'b' data subsets at ∼10 315 μHz or a period of 96.9 s, although the amplitude is very small (∼0.5 mmi); this frequency is just visible in Fig. 3.

Table 3 lists the 24 frequencies extracted from the two half data sets in order of decreasing amplitude in the first ('a') data set; this is not the exact order in which they were detected, because individual sequential frequency extraction and non-linear simultaneous

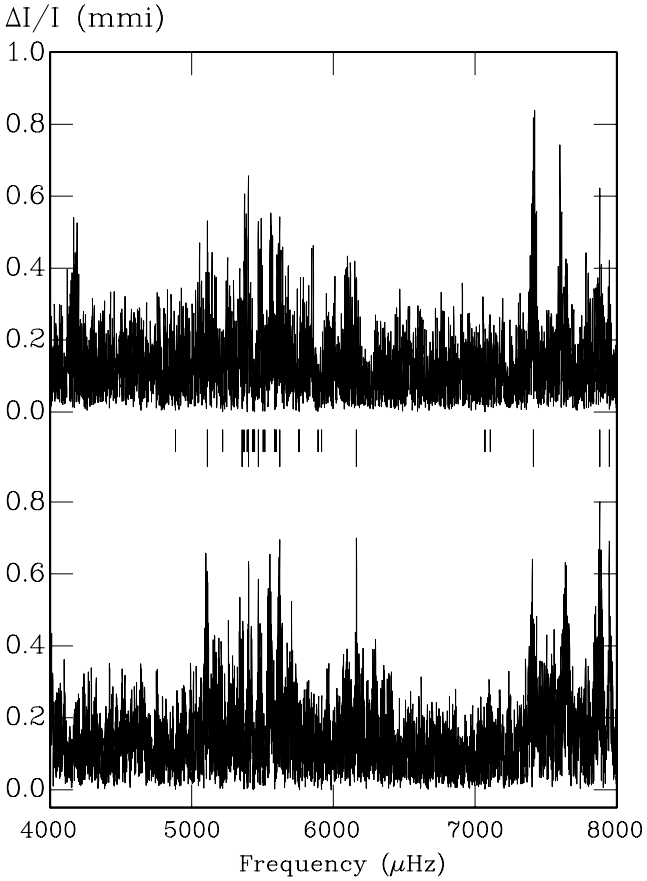

Figure 6. Periodograms (amplitude/frequency) for the first (upper) and second (lower) halves of the Xcov17 photomultiplier data after simultaneous removal of 19 frequencies. In the middle of the figure, the short vertical lines indicate 18 of the first 19 frequencies removed from the full data set; the long vertical lines indicate the nine frequencies subsequently extracted.

extraction can produce slightly different results. Typical formal errors from the simultaneous fitting procedures are about 0.08 mmi in amplitude and range in frequency from about 0.02 μHz for the largest amplitudes to about 0.13 μHz for the smallest, although a better indication of the errors is probably the agreement between the results from the 'a' and 'b' data sets.

The baselines for the half data sets are roughly 6 d or $T \approx 5 \times 10^5$ s. The corresponding resolution for complete separation of two frequencies in such a data set is $\sim 1.5/T$ (Loumos & Deeming 1978) or 2.9 μHz for the half data sets. The quantity $1/T$ (~2 μHz) can be regarded as a reasonable limit, closer than which nearby frequencies would be 'unresolvable', so that we could not expect to separate any frequencies more closely spaced than about 2 μHz. By extension, if frequencies extracted from the two halves of the data are closer than $1/T$, we can say they are formally the same. For all of the frequencies listed in Table 2, the differences between the results from the two half data sets are less than $1/5T$ (0.4 μHz), well within the $1/T$ resolution.

Conversely, there are three very close pairs of frequencies in Table 3 (near 5434, 5586 and 5759 μHz). The first two pairs of these, with separations of 2.5 and 2.7 μHz, are just closer than the formal limit for complete frequency separation and all three could be artefacts – for example, the beat periods of the pairs of frequencies are all around 4 d, so that some instrumental difference causing apparent amplitude variation might result in one period being split into two. It is known that some of the pulsating subdwarfs can have several very close frequencies (Kilkenny et al. 1999) so the reality of the close frequencies in PG 1336−018 cannot be ruled out, but amplitude modulation could also produce such close frequencies.

Table 3. Frequencies, semi-amplitudes (s_a and s_b) and periods derived by simultaneous fitting of all 24 frequencies from the two halves of the Xcov 17 photomultiplier data reduced separately. Typical formal errors are ~0.08 mmi in amplitude and about 0.02–0.13 μHz in frequency.

f_a (μHz)	f_b (μHz)	Δf (μHz)	s_a (mmi)	s_b (mmi)	P_a (s)	P_b (s)
5757.28	5757.32	−0.04	4.8	4.6	173.693	173.692
5585.52	5585.76	−0.24	4.1	3.9	179.034	179.026
5369.42	5369.37	0.05	3.4	3.9	186.240	186.241
5392.19	5392.15	0.04	1.8	2.9	185.453	185.455
5444.31	5444.22	0.09	1.8	1.8	183.679	183.681
5435.56	5435.43	0.13	1.7	2.3	183.974	183.978
5598.64	5598.25	0.39	1.6	1.8	178.615	178.627
5760.73	5760.81	−0.08	1.6	1.7	173.589	173.586
5432.89	5432.92	−0.03	1.2	1.3	184.064	184.063
7071.05	7071.30	−0.25	1.2	1.1	141.422	141.417
5516.69	5516.90	−0.21	1.1	1.0	181.268	181.261
5587.99	5587.81	0.18	1.1	1.0	178.955	178.961
5916.23	5916.46	−0.23	0.9	1.1	169.026	169.020
5356.28	5356.66	−0.38	0.9	0.8	186.697	186.683
5506.22	5505.95	0.27	0.9	0.7	181.613	181.622
5891.54	5891.55	−0.01	0.8	0.9	169.735	169.735
7108.92	7108.95	−0.03	0.7	1.0	140.668	140.668
4885.16	4885.17	−0.01	0.7	0.8	204.702	204.701
5400.79	5400.42	0.37	0.8	0.5	185.158	185.171
7880.90	7880.64	0.26	0.6	0.8	126.889	126.893
5470.70	5470.87	−0.17	0.6	0.7	182.792	182.786
5219.02	5218.68	0.34	0.6	0.6	191.606	191.619
7948.43	7948.24	0.19	0.4	0.7	125.811	125.814
10314.78	10314.97	−0.19	0.4	0.5	96.948	96.946

4.2 Xcov17 photoelectric data as a whole

Next, a periodogram analysis of the Xcov17 core campaign (April 7–21) was carried out and all the frequencies in Table 3 were quickly recovered. In addition, when the data were pre-whitened by those 24 frequencies simultaneously, and a further periodogram determined, there still remained several peaks which appeared significant. The noise in the periodogram, as estimated by the top of the 'grass', appears to be at about the 0.25-mmi level; peaks with a height >0.4 mmi appear significant. However, to be conservative, we have accepted only four more frequencies with amplitudes >0.5 mmi. We also carried out an analysis of all the data (listed in Tables 1 and 2) and recovered the same frequencies. Table 4 lists all 28 frequencies with the additional four frequencies bracketed to indicate that they were not detected independently in the two 'half' analyses. The frequencies are ranked in order of decreasing amplitude and, in what follows, we use the nomenclature f_n to indicate the nth-ranked frequency.

Note that the baseline of the full campaign data set yields $1/T \sim 1$ μHz – twice as good as the 'half' data sets – and we still recover the three closely spaced frequencies mentioned in Section 4.1.

5 RESULTS

5.1 Comparison with the 1996 discovery data

The discovery paper (Kilkenny et al. 1998) reported results from the 1996 observing season for PG 1336−018. In Fig. 7, we reproduce the

Table 4. Periods, frequencies and semi-amplitudes for the main campaign (data in Fig. 2).

Rank	P (s)	f (μHz)	± (μHz)	s (mmi)
18	204.70	4885.135	0.033	0.7
27	195.65	(5111.097)	0.048	0.5
21	191.61	5218.963	0.039	0.6
16	186.69	5356.449	0.032	0.8
3	186.24	5369.369	0.007	3.7
4	185.45	5392.145	0.010	2.5
25	185.15	5400.761	0.046	0.6
10	184.05	5433.175	0.022	1.3
5	183.98	5435.422	0.013	2.0
7	183.68	5444.316	0.015	1.7
22	182.79	5470.859	0.039	0.6
17	181.63	5505.681	0.032	0.8
12	181.27	5516.719	0.026	1.0
2	179.03	5585.657	0.007	4.0
13	178.96	5587.777	0.029	1.0
6	178.62	5598.527	0.016	1.7
20	177.90	(5621.260)	0.038	0.7
1	173.69	5757.304	0.005	4.7
8	173.59	5760.765	0.015	1.7
15	169.74	5891.498	0.029	0.9
11	169.03	5916.264	0.025	1.0
28	162.25	(6163.430)	0.051	0.5
9	141.42	7071.261	0.022	1.3
14	140.67	7108.759	0.029	0.9
23	134.90	(7412.908)	0.042	0.6
19	126.89	7880.963	0.035	0.7
24	125.81	7948.553	0.042	0.6
26	96.95	10314.780	0.054	0.5

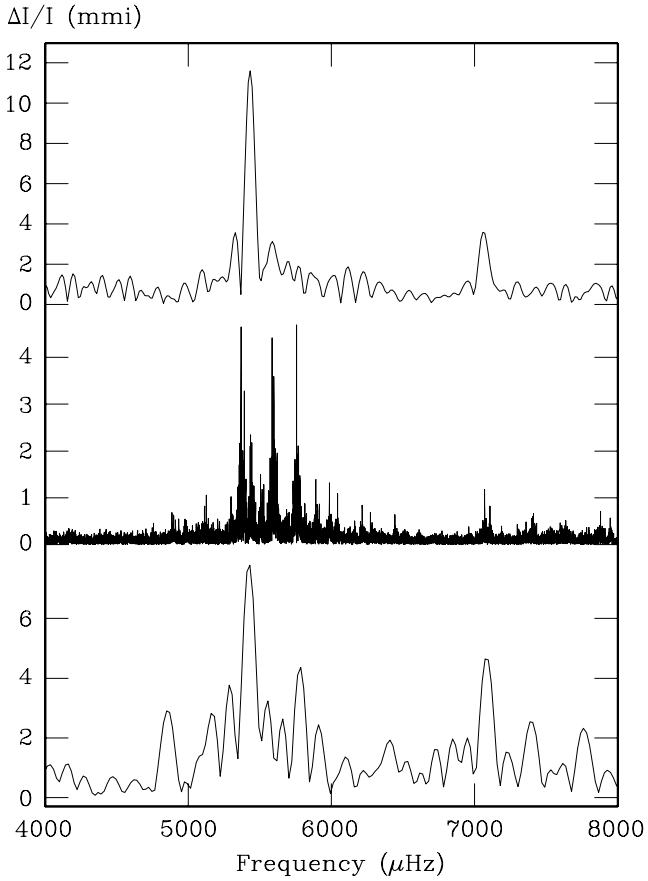

Figure 7. A comparison of the (amplitude/frequency) periodograms for the PG 1336−018 discovery data of 1996 (upper), the Xcov17 core campaign data (middle) and a U-band light curve also obtained in 1996 (lower). The upper and lower figures are taken from Kilkenny et al. (1998), although the amplitude scales have been adjusted to make the comparison of frequencies easier. The vastly better resolution of the middle periodogram is a result of the much longer baseline and high data density and also serves to highlight the value of multisite type campaigns.

periodogram of the discovery light curve (a 5.2-h 'white light' run), the periodogram from the Xcov17 campaign and a periodogram from a 1996 'U'-band light curve. The latter was only a 2.7-h run but has the advantage that it should be relatively unaffected by any light from the much cooler companion.

The main peak in the 1996 data seems to be at 5435 μHz (184.0 s), corresponding to f_5 (or perhaps f_{10}) in the Xcov17 data. The next most significant peak in 1996 was at 7076 μHz (141.3 s) and clearly matches $f_9 + f_{14}$ in the current data. Beyond these two frequencies, little could be deduced from the discovery data, although it was noted that there could well be more frequencies below the 0.003-mag level. In Fig. 7, f_1 is not visible in the 1996 white light data, although there is a weak corresponding peak in the U data; f_2 might have a corresponding peak in the white light data, but is not visible in the U data; and the frequencies f_3 and f_4 (at 5369 and 5392 μHz) are not visible in either set of 1996 data. It is not likely that these effects are a matter of resolution; a 5-h light curve such as the upper part of Fig. 7 will give a frequency resolution of about 55 μHz and the f_1, f_2 and f_3 frequencies are separated by ∼200 μHz. In addition, frequency spectra of the Xcov17 data calculated on a run-by-run or day-by-day basis easily resolve the main frequencies seen in the middle panel of Fig. 7. As examples, Fig. 8 shows consecutive individual observing runs (of reasonable length) where it is clear that the power, at least in the three dominant frequencies, is changing from run to run. Fig. 9 is a similar plot of consecutive runs from a single site. Again it is obvious that the power in the three main peaks changes in a complex manner. The $f1/f2$, $f1/f3$ and $f2/f3$ beat periods are only 1.6, 0.7 and 1.3 h respectively, which makes beating between the largest modes an unlikely explanation. Additionally, with an orbital period of 2.4 h, it is unlikely that structural or temperature variations due to the companion can be the cause (unless they are not tidally locked). One possible explanation would be that these are in fact unresolved peaks in the amplitude spectrum. Although the length of the campaign makes this seem unlikely, similar stars (PG 1605, PB 8783) also show closely spaced peaks – and the barely resolved peaks in our amplitude spectrum (such as $f4$ and $f10$ or $f1$ and $f8$) do not rule out this explanation.

5.2 Rotational splitting of frequencies

In a very close binary system such as PG 1336−018, it is to be expected that the circularization and synchronization times will be very short – of the order of a few decades (Zahn 1977). It is thus reasonable to assume that the orbital period of the system is also the rotation period of the two components of the system. We have searched for frequency differences at the orbital period (0.101016 d) and at half the orbital period – equivalent to 114.576 and 229.152 μHz respectively, and frequency differences near these values are listed in Table 5.

Typical splitting coefficients ($C_{n\ell}$), derived from evolutionary models, for low-order modes appropriate for EC 14026 stars range from 3 to <0.08 per cent Unfortunately, the extracted eclipses

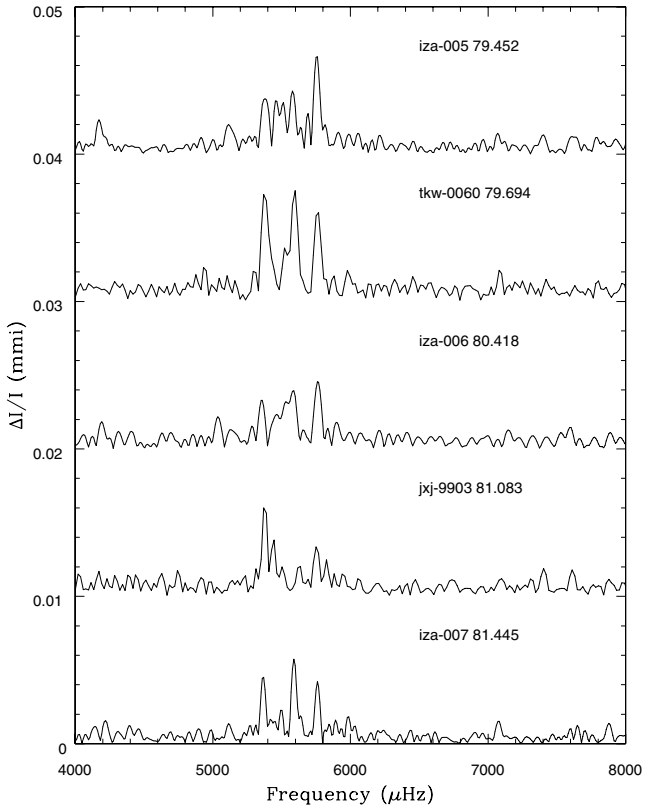

Figure 8. A comparison of the (amplitude/frequency) periodograms for consecutive runs. Each run name is indicated (see Table 1) as well as the run start time from BJED 2451200. The three dominant frequencies are clearly resolved and have variable amplitudes.

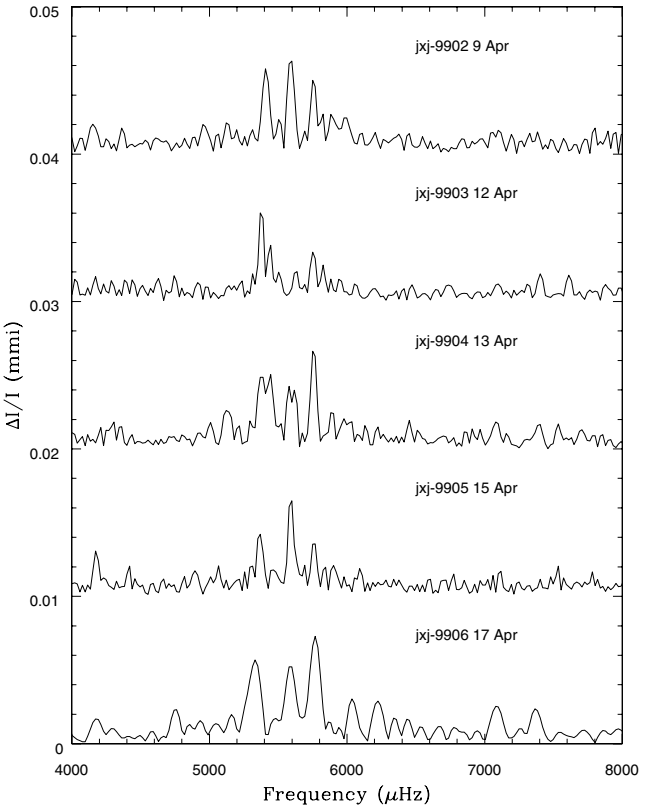

Figure 9. A comparison of the (amplitude/frequency) periodograms for consecutive runs from a single site (BAO). Each run is indicated as well as the run start date.

produce a gap every 114.576 μHz, from which the Fourier transform produces an alias peak (as evident in Fig. 4) at successive overtones of the orbital period (114.576, 229.152, 343.728 μHz, etc.). This makes it extremely difficult to separate real, rotationally split modes from aliases caused by the extracted eclipses. The mode most likely to be rotationally split is f_2–f_3, where the amplitudes are sufficiently large to rule out aliasing and the splitting is far enough away from half the orbital period (∼13 μHz) that it is unlikely to be an alias. The remaining splittings are difficult to justify at best, particularly because one of each pair typically has an amplitude far greater than the other and the low amplitude peak is directly on the alias introduced by cutting out the eclipses.

5.3 Models

Although it is rewarding to resolve the complex pulsations of PG 1336−018 in so much greater detail than previously, the real goal is to compare observed pulsations to model pulsations. It is only through the models that we can hope to understand the internal conditions of sdB stars.

The usual way of comparing a model to observations is by using spectroscopic results as a constraint on $T_{\rm eff}$ and log g and finding those models whose periods are in the same range as observed (see, for example, Kilkenny et al. 2002; O'Donoghue et al. 1998). To narrow the range of models further, it is necessary to have additional constraints, such as an observational way to identify the spherical harmonics of individual modes. This is usually accomplished by using evenly spaced frequencies or periods in the observed amplitude spectrum. For p-mode pulsations (as expected in EC 14026 stars; Charpinet et al. 2001) evenly spaced frequencies can be caused by successive values of the radial order n (sometimes called k) for the same degree index ℓ (however, for low n values, the frequencies will not be split evenly) or by multiplets with the same values of ℓ and n, but differing azimuthal order m. In the latter case, the degeneracy is typically broken by rotation and neighbouring m values are split (to within a few per cent) by the rotation frequency. Thus, for $\Delta m = |1|$, $\Delta f \approx P_{\rm rot}^{-1}$. For PG 1336−018, we assume such constraints a priori.

Because it is in a close binary, we assume it is tidally locked so that we know the rotation period, which provides characteristic frequency splittings to look for. Such splittings (or multiples thereof) would be a sign of rotationally split modes. Because $(2\ell + 1)$ m values are allowed, the number and spacing of such modes would allow ℓ values to be constrained. Such constraints could then be passed on to the model.

To this end, we have computed the pulsation periods of evolutionary models (generated using ISUEVO; Dehner & Kawaler 1995), as

Table 5. Possible rotationally-split frequencies.

Frequency	Δf	$C_{n\ell}$
f_4–f_{17}	113.536	0.009
f_{22}–f_2	114.798	0.002
f_{16}–f_{22}	114.410	0.001
f_{17}–f_{20}	115.579	0.008
f_2–f_3	216.288	0.03
f_3–f_6	229.158	1.3×10^{-5}
f_4–f_{20}	229.115	8.1×10^{-5}
f_{16}–f_2	229.208	1.2×10^{-4}

in Kawaler (1999). Such models are specified by five independent parameters: log g, $T_{\rm eff}$, the core mass $M_{\rm core}$, the mass of the outer hydrogen-rich envelope $M_{\rm env}$, and the metallicity. Ideally, log g and $T_{\rm eff}$ are constrained by spectroscopy and the remaining parameters determined by fitting the periods – as in Kawaler et al. (1995) and independently confirmed using *Hubble Space Telescope* (*HST*) data in Reed, Kawaler & O'Brien (2000), or in Kawaler (1999) and independently confirmed using rotational velocities by Heber, Reid & Werner (2000). However, this only works if it is possible to identify the spherical harmonics of the observed modes (such as the rotationally split modes described above). Otherwise, it is only possible to estimate these parameters based on theory and an approximate fit of the model periods to those observed.

As an illustrative example of this process, we have evolved solar metallicity models off the zero-age extended horizontal branch (ZAEHB) using a fixed core mass of 0.470 $M_\odot$ and varying $M_{\rm env}$ from 0.0000 to 0.0055 $M_\odot$ in steps of 0.0001, keeping only those sequences that match (to within 2σ) the spectroscopic constraints. The vast majority of models within the spectroscopic constraints have periods in the range of those observed. To select from within this group of models, it is necessary to use additional clues from the observations.

We begin by concentrating on the high amplitude periods. As previously noted, the amplitude spectrum of PG 1336−018 is largely dominated by three periods. Of these, two are split by $2f_{\rm orb}$, which would correspond to $\Delta m = 2$. As such, possible values of ℓ and m are $\ell = 1$, $m = +1$, -1; $\ell = 2$, $m = +1$, -1, or $m = 0$, ± 2 – assuming that $\ell > 2$ modes cannot be seen due to geometric cancellation across the surface (Reed et al., in preparation). The remaining mode, f_1, is assumed to be radial as no rotationally split components are detected. Of course, it is possible that f_1 is $\ell \neq 0$, but then the remaining multiplet components would have to be below our detection limit, which is an order of magnitude less than the amplitude of f_1. Because f_2 and f_3 are a rotationally split pair of comparable amplitude, our assumption of $\ell = 0$ for f_1 seems reasonable, and certainly adequate for this example. Among the models available, the model with the closest fit to the observed periods with the above mode constraints has a total mass of 0.4704 $M_\odot$, log $g = 5.726$ and $T_{\rm eff} = 31\,200$ K.

Table 6 shows the pulsation periods for low values of n and ℓ for the p-modes of the best-fitting sdB model. We stress that this is a very preliminary identification; the periods in the table indicate that models of evolved sdB stars can qualitatively reproduce the observed periods. More secure identifications, and therefore constraints on the properties of PG 1336−018, will have to wait until a more exhaustive grid of model parameters, appropriate for this region of the HR diagram, is complete.

Table 6. Pulsation periods of an evolved sdB star with $T_{\rm eff} = 31\,000$ K and log $g = 5.726$. The '†' symbol indicates periods used to constrain the model.

Degree ℓ	Radial index n	Azimuthal order m	Model period (s)	PG 1336 period (s)
1	3	−1	96.0	97.0
1	3	0	97.1	
1	3	+1	98.2	
0	2	0	114.6	
1	2	−1	164.2	162.3
1	2	0	167.3	
1	2	+1	170.6	169.7
0	1	0	174.3	173.7†
2	1	−2	174.9	
2	1	−1	178.5	179.0†
2	1	0	182.2	181.6
2	1	+1	185.9	186.2†
2	1	+2	190.1	191.6
2	0	−2	214.9	

As an additional constraint, we can use the known inclination, $i \approx 81^\circ$, of the orbit; assuming that the pulsation axis is aligned with the rotation axis (as is commonly the case for non-radial pulsation; although a subsequent paper will explore perturbations on this assumption). It can be shown (Dziembowski 1977) that non-radial pulsation amplitudes are proportional to $P_{\ell m}(\cos i)$. For extreme values of i, certain non-radial amplitudes should be unobservable. At $i \approx 81^\circ$, amplitudes for modes with $\ell = 1$, $m = 0$ and $\ell = 2$, $m = \pm 1$ should be reduced by 84 per cent.

This makes it seem unlikely that our identifications for f_2 and f_3 are correct. However, our model is illustrative of the success that can be had in general producing models with pulsation periods in the proper range, and also in the risk of fitting models to observed pulsations without constraints on the spherical harmonics. PG 1336−018 pulsates in 28 modes between 96 and 205 s, while our model can only produce 14 pulsations (11 if the inclination is taken into account). Therefore, without the added constraints provided by our assumed $P_{\rm rot}$ and pulsation inclination, we would have far too many models that fit the observations. In fact, it would be nearly impossible to create a model that matched the spectroscopic constraints but did not fit *some* of the observed periods.

Over 30 pulsating sdB stars have now been detected. Of these, only a few have had their temporal spectrum resolved and within this group only three or four have additional constraints to allow precise modelling. Examples are: PG 1605+072 for which Kawaler (1999) made a model fit; PG 0014+067 for which Brassard et al. (2001) have modelled the 13 observed frequencies; and PG 1047+003 for which Charpinet et al. (2002) have given preliminary theoretical results.

The observations described in this paper (and our preliminary model fit) will hopefully provide a basis for theoreticians to advance their models. In particular, it would be of very great interest to see an application of the Montréal parameter search method to PG 1336−018 (see, for example, Brassard et al. 2001; Charpinet et al. 2002).

5.4 The pulsation spectrum in primary eclipse

Because non-radial pulsations manifest themselves as a geometric effect (alternating hotter and cooler regions on the stellar surface), and because the visible surface area of the sdB pulsator changes during primary eclipse, so might the observed pulsation amplitudes – depending, of course, on the pulsation mode. In principle, we can use these changes to determine what modes are present if we can distinguish real modes from aliased modes during primary eclipse. A substantial problem is that we only have 800 s (∼0.2 h) of eclipse data in every 2.4 h of orbital period. At best, therefore, we can only obtain a data coverage of about 9 per cent of any given baseline. Additionally, the ∼800 s of coverage is only about four or five pulsation cycles, which is very limited, given the number of frequencies detected in the out-of-eclipse data. This means that every real oscillation frequency creates a large and complex assortment of alias peaks in the Fourier transform. This might not be a problem if we had observed all (or most) of the primary eclipses. Unfortunately, during the best 11-d period of the run, we only accumulated 49 per

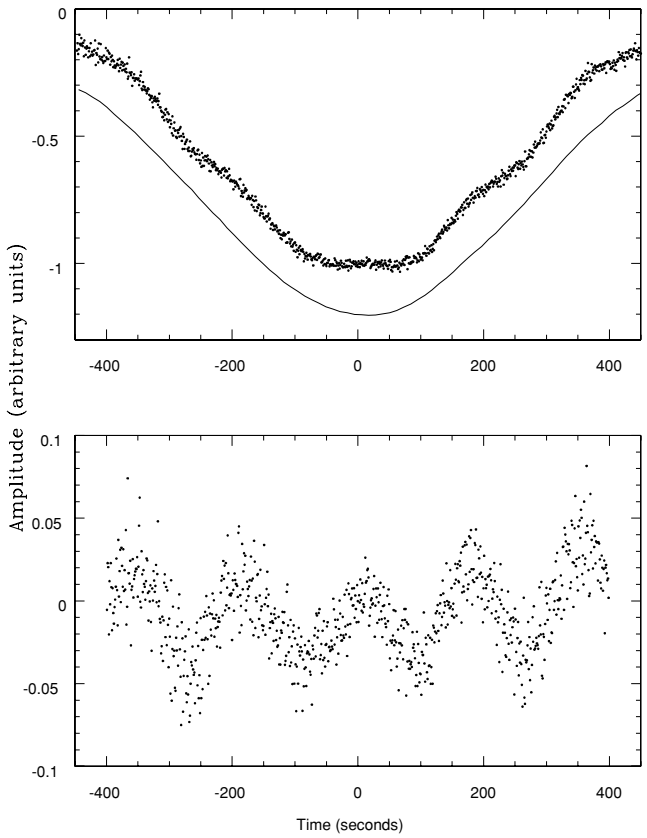

Figure 10. The upper panel shows typical eclipse data with the averaged template or correcting contour (solid line) offset by −0.2. The lower panel shows the same eclipse corrected by the smooth template from the upper panel and showing obvious pulsations.

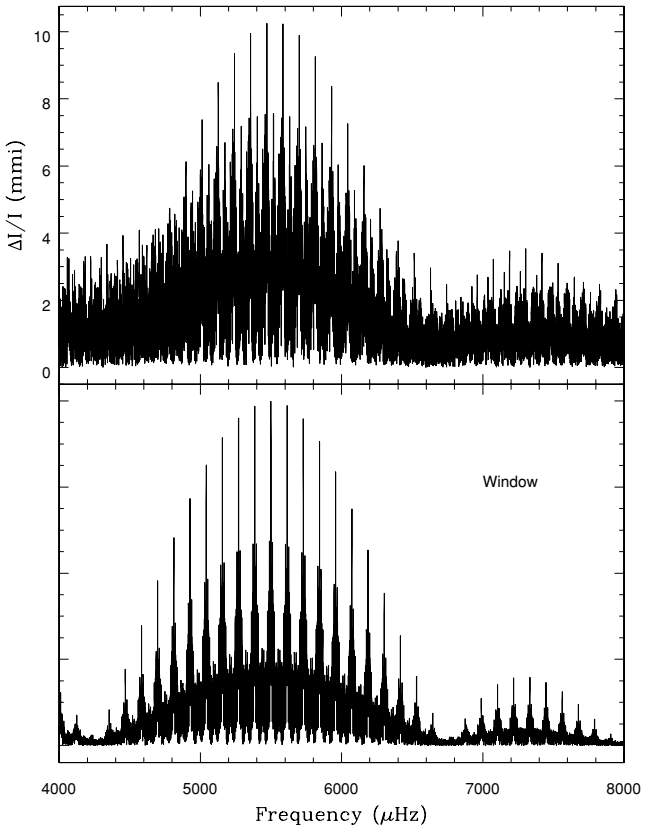

Figure 11. The upper panel shows the Fourier transform of all primary eclipse data. The lower panel shows a data window for the eclipse data.

cent of the primary eclipses, making the gaps even larger – effectively, the eclipse data have only about a 4 per cent coverage of the data baseline.

In order to remove the effect of the eclipse variations, we first extracted all the eclipses and added them together to create a template eclipse in which the pulsation effects have been essentially averaged out (see the upper panel of Fig. 10). The individual eclipses were then divided by the template eclipse, leaving a flattened eclipse (illustrated in the lower panel of Fig. 10). In some cases, a second-order to fourth-order polynomial was also used to remove second-order effects (caused by varying seeing at different sites, for example).

Fig. 11 shows the Fourier transform of all the primary eclipse data along with the data window. There is one very obvious frequency in the eclipse data at 5757 μHz (f_1) and we were able to recover two other frequencies at 5585 and 5505 μHz (f_2 and f_{17}). However, the aliasing was too severe to allow further frequency extraction.

Although these data were insufficient to use eclipse mapping to identify pulsation modes, it does indicate that the method is viable. With less than 40 per cent of the eclipses, we were able to recover the two highest amplitude modes. Simulations suggest that a coverage of around 80 per cent would be sufficient to recover most of the real pulsations.

5.5 Orbital phase shifts

In an earlier paper, Kilkenny et al. (1998) reported an attempt to detect phase shifts in the principal pulsation frequency due to the binary orbit. They found no significant effects and noted that from the light-curve and radial-velocity solution, the light travel time across the orbit was only about 0.9 s – small compared to the errors in the determination of the phase shifts from relatively small blocks of data. They also noted that the secondary pulsation would induce an even bigger (apparent) phase shift into the primary frequency – and the effect would be further complicated if either pulsation had a variable amplitude. Clearly, a much more detailed map of the pulsation frequencies was required, and we now have that.

With the much larger data set at our disposal, we divided the data into eight parts, based on tenths of the orbital phase, $0.05 < \phi < 0.15$, $0.15 < \phi < 0.25$, and so on, but omitting phases 0.45–0.55 and 0.95–0.05 which cover the two eclipses. We tried several solutions, none of them completely satisfactory. It would be preferable to solve for all known frequencies simultaneously, because this reduces the effect that even weak frequencies might have in producing apparent phase shifts in the other frequencies. In practice, this was not possible because, although we tried initially to solve for all 28 frequencies in Table 4, some of the weaker frequencies were consistently missed (or the solution produced a slightly different frequency when 'forced'). It is not hard to see how this happens – with the data restricted to a phase range of only a tenth of the orbit, we have an effective coverage of only about 5 per cent (given that the total coverage is about 47 per cent). In other words, the window function looks like that displayed in the lower panel of Fig. 11, which results from a comparable sample of the total data set. We have tried various solutions with the misidentified frequencies omitted, cutting first to 24 and then 21 frequencies, but none of these was satisfactory. However, although the solved frequencies did vary slightly from attempt to attempt, the frequency differences (between the different

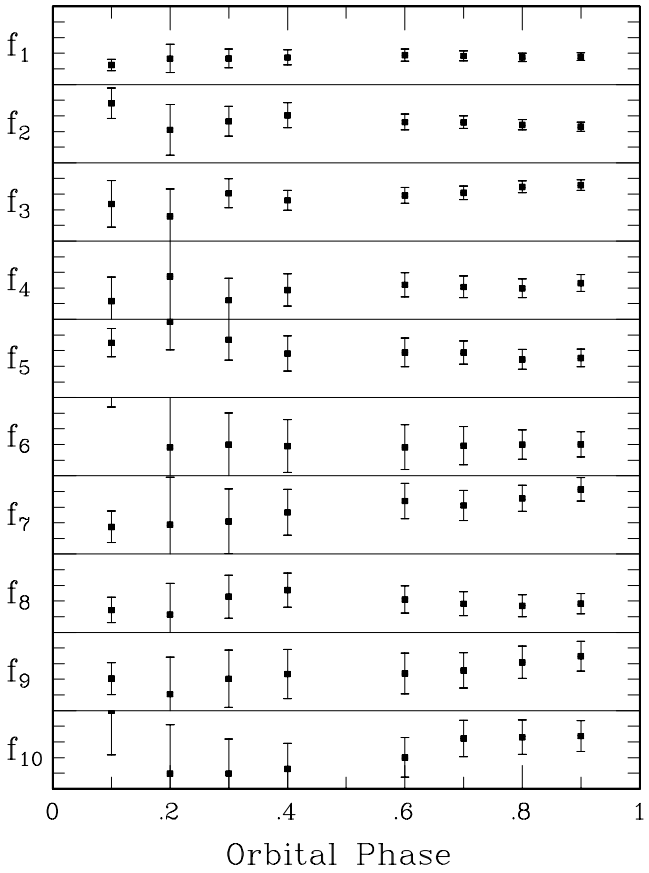

Figure 12. Phase shifts in the 10 strongest frequencies from Table 4 as a function of orbital phase. The ordinate carets are separated by 0.05 rad (1.4 s at 5757 μHz) and the zero point is arbitrary, as we are interested only in phase differences. The error bars indicate the formal 1σ errors of the frequency extraction procedure.

orbital phases) seemed to remain relatively stable. In Fig. 12, we present a solution for the 10 strongest pulsation frequencies, which turn out to be those with amplitudes greater than 1 mmi (actually $\geqslant$1.3 mmi). It is clear that the formal errors in the data points are mostly much larger than the effect we might expect to see from the binary orbit – or any other effect which might be present in the data, because the 10 sets of data shown in Fig. 12 can almost all be fitted with a horizontal straight line which would cut all of the 1σ error bars, implying no significant effect. The weaker frequencies show even less significant results.

The strongest frequency (f_1 at 5757 μHz) has the smallest errors, typically around 0.03 rad, corresponding to a phase shift of about 0.5 per cent, or about 0.8 s in the 173-s pulsation. This is similar to the size of the effect we expect from the binary solution. A formal fit of a sinusoid to the eight orbital phase points results in an amplitude of 0.02 ± 0.007 rad, or a peak-to-peak effect of 0.04 rad, equivalent to 1.1 ± 0.4 s for the light travel time across the orbit. It appears that this result is unduly weighted by the point at phase 0.1; removal of this point results in an amplitude solution of 0.01 ± 0.002 rad, or about 0.6 ± 0.1 s for the orbital size. The errors quoted are the formal errors from the sine fitting, but it seems more reasonable to expect the error to be of the order of the difference between the two solutions.

We have also fitted a sinusoid to all 80 points (10 frequencies at eight orbital phases), weighting the data as $1/\sigma^2$, but the derived amplitudes are negligible – especially for the more realistic solution which satisfies the physical restriction that the phase shifts must be at extrema for orbital phases 0.0 and 0.5 (at the eclipses) when the pulsating star is nearest to and farthest from the observer. It can be seen in Fig. 12 that some of the frequencies seem to show secular trends in phase – but not all in the same direction. Because such trends imply that there is a commensurability between orbit and phase *change*, they are probably not real. This strongly suggests that the formal errors from the frequency extraction process are underestimated and explains why adding in more data points does not improve the errors in the fit.

We have also tried combining the data around orbital phases 0.1 and 0.9, and comparing the pulsation phases to the combined data around orbital phases 0.4 and 0.6. This results in a range of phase differences between effectively zero and about 0.4 rad – no consistent solution emerges. Again the errors are too large.

The above results are rather inconclusive and all of the above solutions will be further confused by the effects of the weaker frequencies and perhaps by any amplitude variations of the kind noted in Section 5.1.

6 SUMMARY

In Section 1, we listed five aims of the current multisite campaign. Only one of these has been attained with the success we had hoped for, although some progress has been made with all.

(i) We have greatly increased the number of known frequencies for the pulsating sdB star, PG 1336−018, from two definite identifications (plus a few suspected at the <3-mmi level) to over 20, possibly as many as 28, identifications down to amplitudes around 0.5 mmi, none of which appears to be a harmonic or sum of other identified frequencies. We have also established not only that the frequency structure has changed markedly since the discovery observations of 1996, but also that this structure appears to change on time-scales comparable with a day. It is not clear at this stage whether this is due to frequencies yet unresolved or to amplitude changes due to some other mechanism.

(ii) A search for rotationally split modes was largely unsuccessful, although f_2 and f_3 might be such a case. With no sign of rotational splitting of the f_1 mode, however, we have assumed this to be a radial mode and f_2 and f_3 to be rotationally split components of a non-radial mode for the purposes of creating a model of the pulsating star.

(iii) Evolutionary models were generated to fit the observed pulsation frequency regime and spectroscopic constraints – as has been done for several other EC14026 stars. The known inclination and assumed tidally locked rotation period provide additional constraints for PG 1336−018. These constraints indicate that our best-fitting model does not adequately describe the pulsation structure of PG 1336−018. None the less, the significant number of frequencies identified by this work, along with the added constraints should provide a useful basis for future modelling attempts.

(iv) We have been successful in extracting pulsational light variations from primary eclipse data (the discovery paper found this impossible from the much smaller data set) but have only been able positively to identify three frequencies – and with insufficient detail to use eclipse mapping to identify actual modes. Simulations (carried out after the campaign) suggest that if 80 per cent of primary eclipses had been observed over the two-week run, rather than 47 per cent, the method would have been much more successful.

(v) For a similar reason, the current data set is too small to allow a direct determination of the orbital size from the pulsation phase

shifts. Certainly, our data agree with the orbital radius determined from the binary solution within the experimental errors, but they are some way from improving on the accuracy of the orbital size (and hence the stellar radii).

ACKNOWLEDGMENTS

SD, SLS and JLD (Visiting Astronomers at the German–Spanish Astronomical Centre, Calar Alto, operated by the Max-Planck-Institut for Astronomy, Heidelberg, jointly with the Spanish National Commission for Astronomy) acknowledge travel grant DR 281/10-1 from the Deutsche Forschungsgemeinschaft. DK thanks Chris Koen for discussion of and assistance with statistical analyses. PM is supported in part by Polish KBN grant 5 P03D 012 020. MDR was partially funded by NSF grant AST9876655 and by the NASA Astrophysics Theory Program through grant NAG-58352 and would like to thank the McDonald Observatory TAC for generous time allocation. OS would like to thank the Spanish DGESIC and Universidade de Vigo Xunt a de Galicia for partly funding his observations at Tenerife (grants PB97-1435-C02-02 and 64502C844). DJS thanks the MSSSO Time Allocation Committee for the observing time at Siding Spring, the University of Canterbury for the observing time at Mt. John, and the IITAP at Iowa State University for some travel support.

We are grateful to an anonymous referee for suggestions which we believe have strengthened the paper.

REFERENCES

Brassard P., Fontaine G., Billères M., Charpinet S., Liebert J., Saffer R. A., 2001, ApJ, 563, 1013
Charpinet S., Fontaine G., Brassard P., 2001, PASP, 113, 775
Charpinet S., Fontaine G., Brassard P., 2002, in Aerts C., Bedding T.R., Christensen-Dalsgaard J., eds, ASP Conf. Ser. Vol. 259, Radial and Non-Radial Pulsations as Probes of Stellar Physics. Astron. Soc. Pac., San Francisco, p. 364
Charpinet S., Fontaine G., Brassard P., Chayer P., Rogers F. J., Iglesias C. A., Dorman B., 1997, ApJ, 483, L123
Deeming T. J., 1968, Vistas in Astron., 10, 125
Deeming T. J., 1975, Ap&SS, 36, 137
Dehner B. T., Kawaler S. D., 1995, ApJ, 445, 141
Drechsel H. et al., 2001, A&A, 379, 893
Dziembowski W., 1977, Acta Astron., 27(3), 203
Green R. F., Schmidt M., Liebert J., 1986, ApJS, 61, 305
Heber U., Reid I. N., Werner K., 2000, A&A, 363, 198
Kawaler S. D., 1999, in Solheim J. E., Meištas E. G., eds, ASP Conf. Ser. Vol. 169, Proc. 11th European White Dwarf Workshop. Astron. Soc. Pac., San Francisco, p. 1
Kawaler S. D. et al., 1995, ApJ, 450, 350
Kazarovets E. V., Samus N. N., Durlevich O. V., 2000, IBVS, 4870, 1
Kilkenny D., 2002, in Aerts C., Bedding T. R., Christensen-Dalsgaard J., eds, ASP Conf. Ser. Vol. 259, Radial and Non-Radial Pulsations as Probes of Stellar Physics. Astron. Soc. Pac., San Francisco, p. 356
Kilkenny D., O'Donoghue D., Koen C., Lynas-Gray A. E., van Wyk F., 1998, MNRAS, 296, 329
Kilkenny D. et al., 1999, MNRAS, 303, 525
Kilkenny D., Keuris S., Marang F., Roberts G., van Wyk F., Ogloza W., 2000, Observatory, 120, 48
Kilkenny D. et al., 2002, MNRAS, 331, 399
Kurtz D. W., 1985, MNRAS, 213, 773
Loumos G. L., Deeming T. J., 1978, Ap&SS, 56, 285
Menzies J. W., Marang F., 1986, in Hearnshaw J. B., Cottrell P. L., eds, IAU Symp. 118, Instrumentation and Programmes for Small Telescopes. Reidel, Dordrecht, p. 305
Nather R. E., Winget D. E., Clemens J. C., Hansen C. J., Hine B. P., 1990, ApJ, 361, 309
O'Donoghue D. et al., 1998, MNRAS, 296, 296
Reed M. D., Kawaler S. D., O'Brien M., 2000, ApJ, 545, 429
Winget D. E. et al., 1991, ApJ, 378, 326
Winget D. E. et al., 1994, ApJ, 430, 839
Wood J. H., Zhang E.-H., Robinson E. L., 1993, MNRAS, 261, 103
Zahn J.-P., 1977, A&A, 57, 383

This paper has been typeset from a TEX/LATEX file prepared by the author.